Comparison of Hydrodynamic Behavior inside Bed Zone with Non-Simplified and Simplified Air Distributor in a Bubbling Fluidized Bed Gasifier Model

Pinchookorn Chobthiangtham[1,2], Suneerat Fukuda[1,2,*] and Pornpote Piumsomboon[3]

[1]The Joint Graduate School of Energy and Environment, King Mongkut's University of Technology Thonburi, Bangkok, Thailand
[2]Center for Energy Technology and Environment, Ministry of Education, Bangkok, Thailand
[3]Fuels Research Center, Department of Chemical Technology, Faculty of Science, Chulalongkorn University, Bangkok, Thailand
[*]Corresponding author: Tel.: 66-2-8729014-5 #4148, Fax: 66-2-8726978, E-mail address: suneerat@jgsee.kmutt.ac.th

Abstract: The computational fluid dynamic codes of Euler-Euler approach with KTGF were used to develop three-dimensional simulation models to explain the hydrodynamic behaviors of a bubbling fluidized bed gasifier (BFBG). The input parameters and optional model used for the simulation were studied and validated under cold flow (ambient temperature and non-reactive) condition with the experimental results of a downscale BFBG made of acrylic glass. With appropriate input parameters and models, the hydrodynamic behaviors under cold flow condition inside bed zone of BFBG with non-simplified (actual configuration) and simplified air distributor model were compared. The simulation of both non-simplified and simplified air distributor model showed the occurrence of bubbles formation and motion. However, a degree of differences of hydrodynamic behaviors was found between these two models, including the rate of bubble formation and motion inside bed zone, gas-solid flow pattern, bed expansion ratio, and profiles of absolute pressure along the height of bed zone.

Keywords: Computational Fluid Dynamic (CFD); Hydrodynamic Behavior; Bubbling Fluidized Bed Gasifier (BFBG); Simplified Air Distributor.

1. Introduction

It is well-known that the quality and the quantity of gas product from bubbling fluidized bed gasification (BFBG) are dependent on a number of factors including type of biomass, operating condition and system configuration. All these factors affect the chemical reactions as well as the flow characteristics inside the system. Mathematical model simulations have been carried out understand the flow patterns and fluidization process in both macro- and micro-level. Computational fluid dynamics (CFD) codes have also continuously been developed to investigate the thermodynamics and hydrodynamics behavior of flow and reaction systems.

Fluidized bed models are divided into two main categories, i.e., discrete element method (DEM) and two-fluid model (TFM) [1-2]. The DEM, which is based on molecular dynamics, is a simple numerical model by which interactions from multi-body collisions can be calculated. It is also called Euler-Lagrange approach. In this model, the fluid phase is treated as a continuum, while the particles are traced individually. This model has been used for investigating inter-particle force effect on fluidization characteristics [3-4], mixing and segregation characteristics [5-6], particle residence time [7], and minimum fluidization velocity [8] in the bubbling fluidized bed. For the TFM, which is also called Euler-Euler approach, all phases are considered to be continuous and fully interpenetrating. As a bubbling fluidized bed behaves like a chaos motion of a large numbers of particles in the bed, many computational practices present that the DEM will normally take more computational time than the TFM [9, 10]. Furthermore, the TFM is more convenient to facilitate quantifiable decisions for an engineering design as it is able to obtain the mean particulate flow fields. Computational simulations which were done by several groups have been shown feasible to compute the observed bubbles and the flow regime by using TFM. Dig and Gidaspow [11] found that the model based on TFM predicts well the time-averaged and instantaneous porosity in two-dimensional bubbling fluidized beds. Gamwo et al. [12] also found that TFM predicts well the solids flow pattern and the axial solids velocity profiles in a bubbling fluidized bed.

To improve the description of particle collision, the kinetic theory of granular flow (KTGF) has been introduced into the TFM. The kinetic theory formulation includes an interaction term between gas turbulence and particle fluctuations in the granular temperature equation [13]. Enwald and Almstedt [14] found that the KTGF approach for granular flow allows the determination of the pressure and viscosity of the solid in place of empirical relations. Yu et al. [1] developed a new numerical model based on the TFM including the KTGF and complicating reactions to simulate the comprehensive model of BFBG and found that the flow behaviors of gas and solid phases in the bed and freeboard could be predicted and the calculated results of exit gas composition were in agreement with the experimental data.

In most studies of fluidised bed simulation, the uniform air inlet velocity was used by assuming no air distributor for the sake of gas and solid fully mixing [1, 15-16], while Chalermsinsuwan et al. [17] applied a non-uniform parabola inlet velocity profile into the gasifier, which the average inlet velocities were determined from the experimental values. Some studies applied a simplified air distributor model. Papadikis et al. [18] flew the gas through a porous plate at the bottom of the gasifier. Sofialidis and Faltsi [19] simplified the network of horizontal pipes of air distributor as plane circular holes at the gasifier bottom due to the meshing economy reason. Nevertheless, computer efficiency and CFD codes have recently been so much advanced that has enabled simulations of complicating configurations like those of air distributors. By simulating with its full existence, the obscurity inside the bed zone can be clearly investigated, which can be useful for further improvement of air distributor.

In this study, a cold-flow (ambient temperature and non-reactive) simulation of a 100 kWth lab-scale BFBG was carried out using ANSYS FLUENT (formerly FLUENT), a commercial CFD software based on the finite volume method. The model was constructed on three-dimensional (3-D) computational domains and applied the Euler-Euler approach with KTGF. The aim of study was to compare the hydrodynamic behaviors inside the bed zone of non-simplified (actual configuration) air distributor

and the simplified air distributor model. The bubble formation and motion inside bed zone as well as the resulted bed expansion ratio and pressure profile were investigated. Initially, a simple model simulating a downscale transparent bubbling fluidized bed reactor made from acrylic glass was also carried out to validate the model input parameters.

2. Experimental Equipment

Two types of experimental equipment were used in this study: the atmospheric-pressure bubbling fluidized bed gasifier (BFBG) for the cold flow simulation and the downscale transparent bubbling fluidized bed reactor made from acrylic glass for an initial validation of input parameters for the model.

2.1 The atmospheric-pressure bubbling fluidized bed gasifier (BFBG)

The BFBG was developed at JGSEE laboratory and has been used in a number of gasification studies [20-21]. The schematic diagram of the BFBG is shown in Figure 1. It has an internal diameter of 300 mm and a height of 2500 mm with a wall of thermal insulation 150 mm thick. Its lower part situates the nozzle-type air distributor, which consists of 9 closed-end nozzles. Each of them has 42 air distributing holes with 3 mm diameter and 60 degree downward inclination. This air distributor configuration was designed to promote the recirculation of gas and solid in the bed zone and to prevent bed aggregation. Bed material used was silica sand with a mean particle diameter of 0.352 mm and a density of 2647 kg/m^3, which falls into the Group B of Geldart classification. A static height of the bed material was 300 mm.

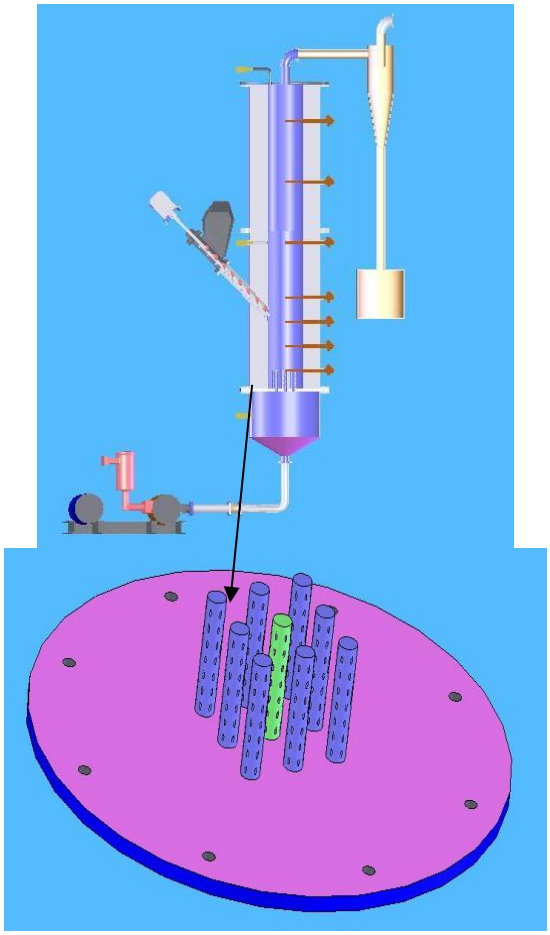

Figure 1. The schematic diagram of bubbling fluidized bed gasifier (up) and 3-D view of air distributor part (down).

2.2 The acrylic bubbling fluidized bed reactor

In order to make an initial validation of the input parameters for the model, a simple model simulating a downscale transparent bubbling fluidized bed reactor made from acrylic glass was also carried out. Visual observation and more thorough pressure measurement could be made and the results were compared with the simulation values. The acrylic reactor was designed to have the ratio of diameter to height the same as that of the BFBG used in this study, i.e. about 1:8, as shown in Figure 2. A series of manometers were installed to monitor the absolute pressure along the height with more frequent positions around the bed zone (every 50 mm from the air distributor level). The silica sand with the same properties as used in BFBG was patched to be 150 mm high. The air distributor was designed to be a plate with 9 distributed holes, below which was fitted by a wire mesh. This simplifies the nozzle-type air distributor in the BFBG. Fluidizing air flow was supplied from a ring blower and controlled by a bypass valve with an air flow meter.

The pressure drop across the bed at minimum fluidization velocity, the bubble appearance inside the bed zone, gas-solid flow pattern and the bed expansion ratio were investigated. The pressure drop across the bed at minimum fluidization velocity was obtained from the graph plot between air velocity and pressure drop across the bed. The bubble appearance inside bed zone and the movement of bed could be visually recorded. The bed expansion ratio was calculated by dividing the quasi-steady state bed height with initial bed height (Hi/H0) [17]. The bed expansion ratio is an important parameter as it is normally used for fixing the height of fluidized bed required for a particular service [22]. The experimental results were then compared with the simulation values.

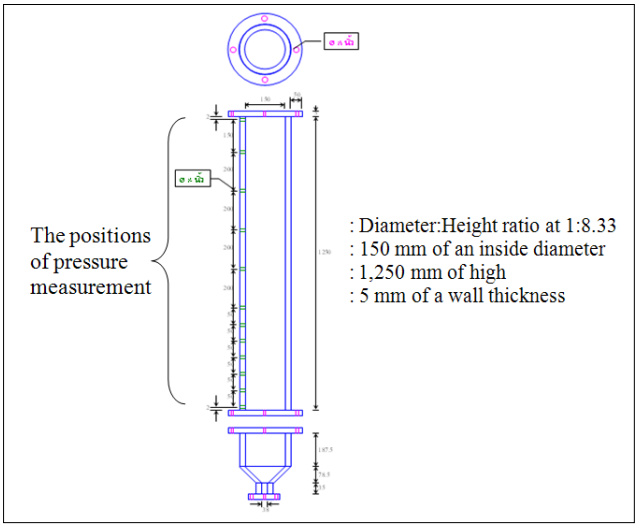

Figure 2. The acrylic bubbling fluidized bed reactor.

3. Simulation Setup

ANSYS FLUENT was used for model simulation throughout this study. The simulations were carried out in three-dimensional (3-D) computational domains under cold-flow condition.

3.1 Computation fluid dynamic model setup

The main conservation equations, which are closed by providing constitutive equations based on the kinetic theory of granular flow (KTGF) as reviewed by many researchers [13, 17, 23-24], were applied in this study.

3.1.1 Mass conservation equations

The accumulation of mass in each phase is balanced by the convective mass fluxes.

$$\frac{\partial}{\partial t}(\propto_g \rho_g) + \nabla \cdot (\propto_g \rho_g \vec{v}_g) = 0 \quad (1)$$

$$\frac{\partial}{\partial t}(\propto_s \rho_s) + \nabla \cdot (\propto_s \rho_s \vec{v}_s) = 0 \quad (2)$$

where α, ρ, and $\vec{v}$ represent the volume fraction, density, and instantaneous velocity and subscripts g, s denote the gas phase and solid phase, respectively.

The summation of all volume fractions is unity as each computational cell is shared by the inter-penetrating phases.

$$\propto_g + \propto_s = 1 \quad (3)$$

3.1.2 Momentum conservation equations

The accumulation of momentum in each phase is balanced by the convective momentum fluxes and the related forces inside the system, i.e. the force due to pressure, stress tensor, gravity, and momentum interphase exchange coefficient

$$\frac{\partial}{\partial t}(\propto_g \rho_g \vec{v}_g) + \nabla \cdot (\propto_g \rho_g \vec{v}_g \vec{v}_g) = -\propto_g \nabla P_g + \nabla \propto_g \cdot \tau_g + \propto_g \rho_g g - \beta_{gs}(\vec{v}_g - \vec{v}_s) \quad (4)$$

$$\frac{\partial}{\partial t}(\propto_s \rho_s \vec{v}_s) + \nabla \cdot (\propto_s \rho_s \vec{v}_s \vec{v}_s) = -\propto_s \nabla P_s + \nabla \propto_s \cdot \tau_s + \propto_s \rho_s g + \beta_{gs}(\vec{v}_g - \vec{v}_s) \quad (5)$$

where P, τ, g, and β_{gs} represent the pressure, stress tensor, gravity force, and interphase exchange coefficient, respectively.

3.1.3 Solid fluctuating kinetic energy conservation equation

The equation of conservation of the solids fluctuating energy is given as

$$\frac{3}{2}\left[\frac{\partial}{\partial t}(\propto_s \rho_s \theta) + \nabla \cdot (\propto_s \rho_s \vec{v}_s \cdot \theta)\right] = -(P_s I + \propto_s \tau_s) : \nabla \vec{v}_s + \nabla \cdot K_s \nabla \theta - \gamma \quad (6)$$

where $(P_s I + \propto_s \tau_s) : \nabla \vec{v}_s$ is the generation of the fluctuating energy due to work done by shear stress in solid phase; $\nabla \cdot K_s \nabla \theta$ is the conduction of the solid fluctuating kinetic energy; γ is the rate of dissipation of the solid fluctuating kinetic energy due to inelastic collision.

Under cold flow simulation, the system can be assumed to be isothermal, hence the energy conservation can be ignored [17].

3.1.4 Constitutive equations

The constitutive equations, based on the KTGF, which have been used to close the conservation equations, are presented as follows:

The stress tensor τ_g and τ_s are given by

$$\tau_g = \mu_g \left[\nabla \vec{v}_g + \left(\nabla \vec{v}_g{}^T\right)\right] - \frac{2}{3} \propto_g \mu_g (\nabla \vec{v}_g) \quad (7)$$

$$\tau_g = \mu_s \left[\nabla \vec{v}_s + \left(\nabla \vec{v}_s{}^T\right)\right] - \frac{2}{3} \mu_s (\nabla \vec{v}_s) + \lambda_s \cdot \nabla \vec{v}_s \quad (8)$$

Here λ_s is bulk viscosity, which is based on expression given by Lun et al. [25] and it can be defined as

$$\lambda_s = \frac{4}{5} \propto_s \rho_s d_s g_0 (1 - e) \left(\frac{\theta_s}{\pi}\right)^{1/2} \quad (9)$$

$$\lambda_s = \frac{\mu_{s,dil}}{(1+e) g_0}\left[1 + \frac{4}{5}(1+e) g_0 \propto_s\right]^2 + \frac{4}{5} \propto_s{}^2 \rho_s d_s (1 + e) g_0 \left(\frac{\theta_s}{\pi}\right)^{1/2} \quad (10)$$

$$\mu_{s,dil} = \frac{5\sqrt{\pi}}{96} \rho_s d_s \theta^{1/2} \quad (11)$$

where $\mu_{s,dil}$ is the dilute viscosity, e is the particle-particle restitution coefficient, and g_0 is the radial distribution function expressing the statistics of the spatial arrangement of particles.

$$g_0 = \left[1 - \left(\frac{a_s}{a_{s,max}}\right)^{1/3}\right]^{-1} \quad (12)$$

where $\propto_{s,max}$ is the volume fraction of the solid phase at maximum packing.

The granular temperature θ_s is defined as

$$\theta_s = \frac{1}{3} \vec{v}_s{}'^2 \quad (13)$$

where $\vec{v'}_s$ is the solids fluctuating velocity.

The solid pressure represents the particle normal forces due to particle–particle interaction. In this approach, both the kinetic and the collisional influence are taken into account. The kinetic portion describes the influence of particle translations, whereas the collisional term accounts for the momentum transfer by direct collisions [13]. The solid pressure is calculated as follows:

$$p_s = \propto_s \rho_s \theta [1 + 2 g_0 \propto_s (1 + e)]^2 \quad (14)$$

The granular conductivity (K_s) and the collisional rate of energy dissipation per unit volume (γ) are adopted as:

$$K_s = \frac{2 K_{dil}}{(1+e) g_0}\left[1 + \frac{6}{5}(1+e) g_0 \alpha_s\right]^2 + 2 \propto_s^2 \rho_s d_s \left(\frac{\theta}{\pi}\right)^{1/2} \quad (15)$$

$$K_{dil} = \frac{75\sqrt{\pi}}{384} \rho_s d_s \theta^{1/2} \quad (16)$$

$$\gamma = 3(1 - e^2) \propto_s^2 \rho_s g_0 \theta \left[\frac{4}{d_s}\left(\frac{\theta}{\pi}\right)^{1/2} - \nabla \cdot v_s\right] \quad (17)$$

In order to couple the two momentum balances in Equation (4) and (5), a model for the interphase force is required. For α_g, the pressure drop due to friction between gas and solid can be described by the Ergun equation. Thus, the interphase momentum transfer coefficient (interphase exchange coefficient), β_{gs}, in this porosity range [27-28] becomes:

$$\beta_{gs} = 150 \frac{\alpha_s^2 \mu_g}{\alpha_g d_s^2} + 1.75 \frac{\rho_g \alpha_s |\vec{v_g} - \vec{v_s}|}{d_s} \quad (18)$$

for $\alpha_g > 0.8$, such a relation for pressure drop leads to the following expression for the interphase momentum transfer coefficient:

$$\beta_{gs} = \frac{3}{4} C_d \frac{\alpha_s \alpha_g \rho_g |\vec{v_g} - \vec{v_s}|}{d_s} \alpha_g^{-1.65} \quad (19)$$

where the drag coefficient C_d is given by

$$C_d = 0.44; \quad \text{for } Re_s > 1000 \quad (20)$$

$$C_d = \frac{24}{Re_s}\left(1 + 0.15 Re_s^{0.687}\right); \quad \text{for } Re_s \leq 1000 \quad (21)$$

where Re_s is the Reynolds number,

$$Re_s = \frac{\alpha_g \rho_g d_s |\vec{v_g} - \vec{v_s}|}{\mu_g} \quad (22)$$

3.2 Simulation setup for validation of model input parameters with acrylic reactor

The Acrylic model (simulating the acrylic reactor) was constructed to validate all the parameters and optional models selected as inputs for ANSYS FLUENT. Following the dimension of acrylic reactor, as shown in Figure 2, the grids were created and meshed in ANSYS Workbench by using DesignModeler and Meshing function, respectively. Then the meshed model was exported from ANSYS Workbench to ANSYS FLUENT for simulation. The boundaries of Acrylic Model were set as presented in Figure 3.

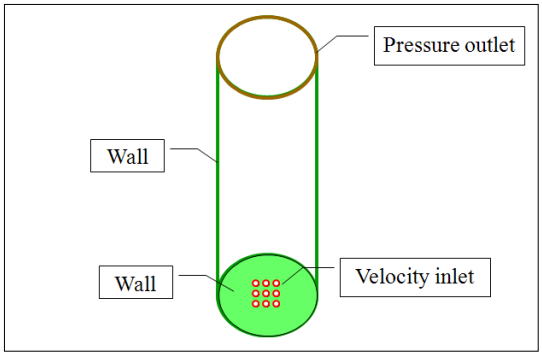

Figure 3. Boundary setting of the Acrylic Model.

The solid phase was silica sand with the same properties and amount to give the same height as that used as a bed material in the acrylic reactor. The momentum-shear condition and the multiphase-granular condition of the solid phase, which was set in a wall boundary, were adjusted following the nature of its behavior according to the previous literatures [29-30]. As the particle of sand was pushed by the air force, it collided with other particles around it. Taking into account this so-called inelastic collision, the optimized value of restitution coefficient in this model was found at 0.9. During the collision, some part of energy was lost and there were a high solid concentration near the wall which prefers a small value of specularity coefficient as found from literatures [31-32]. Here, the optimized value of specularity coefficient was found at 0.01.

For gas phase, the input properties of air used were the same as those used as a gasification medium in the acrylic reactor. The minimum fluidization velocity of 0.206 m/s obtained from equation (23) was also set as the inlet velocity.

$$\boldsymbol{U_{mf} = 0.00114 \frac{g d_s^2 (\rho_s - \rho_g)}{\mu_g}} \quad (23)$$

where $\boldsymbol{d_s}$ is a diameter of particle in solid phase (m), $\boldsymbol{\rho_s}$ is a density of particle in solid phase (kg/m3), $\boldsymbol{\rho_g}$ is a density of gas in gas phase (kg/m3), and $\boldsymbol{\mu_g}$ is a gas viscosity (kg/m-s).

The Gidaspow model was used to represent the terms of interphase exchange coefficient $\boldsymbol{\beta_{gs}}$ for granular flows in this study as it is recommended for dense fluidized beds. It can be written in the following general form:

$$\boldsymbol{\beta_{gs} = \frac{\alpha_s \rho_s f}{\tau_s}} \quad (24)$$

where f is the drag function, and $\boldsymbol{\tau_s}$ is the particulate relaxation time which is defined as

$$\boldsymbol{\tau_s = \frac{\rho_d d_s^2}{18 \mu_g}} \quad (25)$$

where $\boldsymbol{d_s}$ is the diameter of particles.

3.3 Simulation setup for bubbling fluidized bed gasifier with simplified and non-simplified air distributor model

The BFBG Model was constructed to simulate the bubbling fluidized bed gasifier with its actual nozzle-type configuration of the air distributor (non-simplified model) and with a plate-type configuration of air distributor (simplified model). The 3-D drawings showing the cross-section plane of both models are shown in Figure 4. The boundary conditions were set following Figure 3. The input parameters and optional models, which had been studied and validated in the section above, were set as summarized in Table 1.

Table 1. The input parameters for cold-flow simulation.

Problem Setup	Input Parameter
Solver	
Type	Pressure-Based
Velocity Formulation	Absolute
Time	Transient
Model	
Eulerian	2 Phases
Materials	
Air Density (ρ_g)	1.225 kg/m^3
Air Viscosity (μ_g)	1.7893 e-05 kg/m-s
Silica Sand Density (ρ_s)	2647 kg/m^3
Diameter of Silica Sand (d_s)	0.352 mm
Phases	
Primary Phase	Air
Secondary Phase	Silica Sand
Phase Interaction	
- Drag Coefficient	Gidaspow
- Collisions	0.9 (Constant)
Boundary Conditions	
For "Wall" set "Silica Sand"	
- Restitution Coefficient between Silica Sand and Wall (e_w)	0.9
- Specularity Coefficient ($ø$)	0.01
For "Velocity Inlet" set "Air"	
- Air Inlet Velocity (v_g)	3.8137 m/s
Patch	
Phase	Silica Sand
Initial Bed Height (H_0)	300 mm
Initial Solid Volume Fraction (ε_s)	0.538
Solid Inlet Volume Fraction at Maximum Packing Limit ($\varepsilon_{s,max}$)	0.63
Run Calculation	
Time Step Size	0.0001 s
Iterations per Time Step	50

4. Results and Discussion

4.1 CFD model validation

For CFD model validation, the acrylic model simulation results were compared with the experimental results obtained from the acrylic reactor in terms of the pressure drop across the bed at minimum fluidization velocity, the solid volume fraction which represents the bubble appearance inside bed zone and the bed expansion ratio.

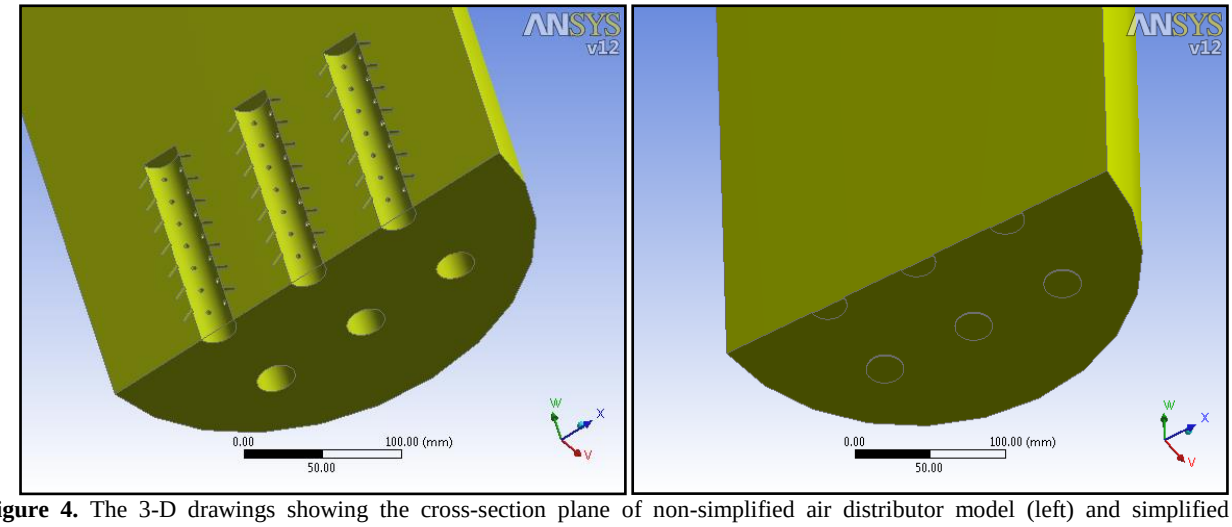

Figure 4. The 3-D drawings showing the cross-section plane of non-simplified air distributor model (left) and simplified air distributor model (right).

4.1.1 The pressure drop across the bed at minimum fluidization velocity

For acrylic model simulation, the pressure drop across the bed at a given minimum fluidization velocity was obtained by the difference between the absolute pressure at the height over bed zone (i.e. around 200 mm from the air distributor level) and that at the air distributor level. The given minimum fluidization velocity was 0.206 m/s, which was obtained from calculation (equation (3.23)). From Figure 5, the simulation gave the absolute pressure at the height of 0 and 200 mm from the air distributor level of acrylic model were 103449 and 101325 Pa, respectively, and hence the pressure drop across the bed of 2124 Pa or 21.66 cm water gauge (cm w.g.). It is also known that, at the minimum fluidization velocity, all the particles are essentially supported by the air stream and the pressure drop through the bed is equal to the bed weight divided by the cross-sectional area of the bed, $\Delta P = W/A$. Based on the weight of sand used of around 4 kilograms in this study, the theoretical pressure drop calculated from this equation was around 2220.53 Pa or 22.64 cm w.g. Yang [33] found that in actual practice, the pressure drop at minimum fluidization velocity would actually be less than W/A because a small percentage of the bed particles is supported by the wall owing to the less than perfect design of the air distributor, to the finite dimension of the containing vessel, and to the possibility of channeling.

In the experiment part, the pressure drop across the bed at minimum fluidization velocity was obtained from the graph plot between pressure drop across the bed and air velocities, as seen in Figure 5. The pressure drop across the bed increased constantly with the increase of air velocity. At the air velocity at around 0.218 m/s, the pressure drop across the bed reached 21 cm w.g., after which was maintained at 20.5 cm w.g. The minimum fluidization velocity was taken at 0.218 m/s where the pressure drop across the bed reached its highest level. The obtained experimental and simulation results of pressure drop across the bed seem to agree well.

4.1.2 The bubble appearance inside bed zone

The visual observation of particle behavior during cold flow experiment in the acrylic reactor was continuously recorded. The captured pictures of the solid bed movement were compared with the contour of solid volume fraction resulted from the acrylic model simulation as a function of time as presented in Figure 6. The movement of contour of solid volume fraction in the acrylic model simulation and of air bubbles in the acrylic reactor coincided well during the simulation time of 0 to 0.6 s.

4.1.3 The bed expansion ratio

The bed expansion ratio was calculated by dividing the quasi-steady state bed height with initial bed height (Hi/H0). The quasi-steady state bed height obtained from simulation was about 170 mm, while it was fluctuating in the range of 170 - 180 mm in acrylic reactor. Based on the same initial bed height of 150 mm, the bed expansion ratios were similar.

From the comparisons of results from experiments and simulation above, it was ensured that the selected input parameters and optional model were acceptable for the simulation to investigate the effect of the air distributor configuration.

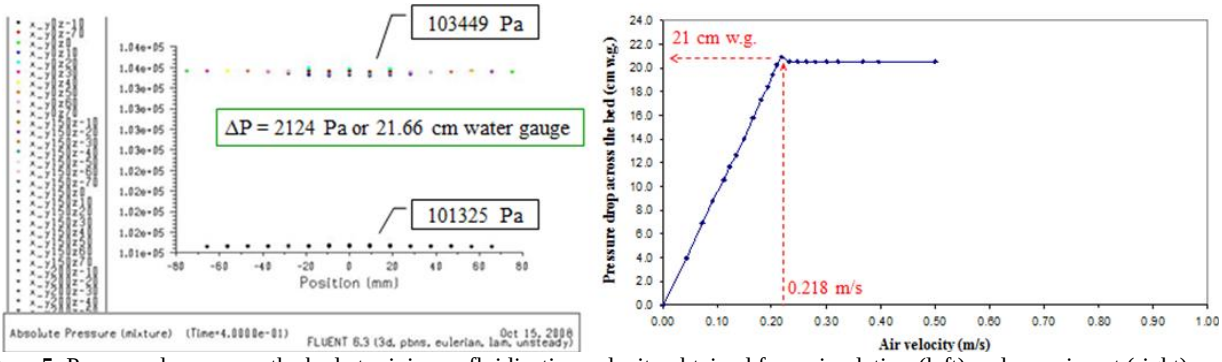

Figure 5. Pressure drop across the bed at minimum fluidization velocity obtained from simulation (left) and experiment (right).

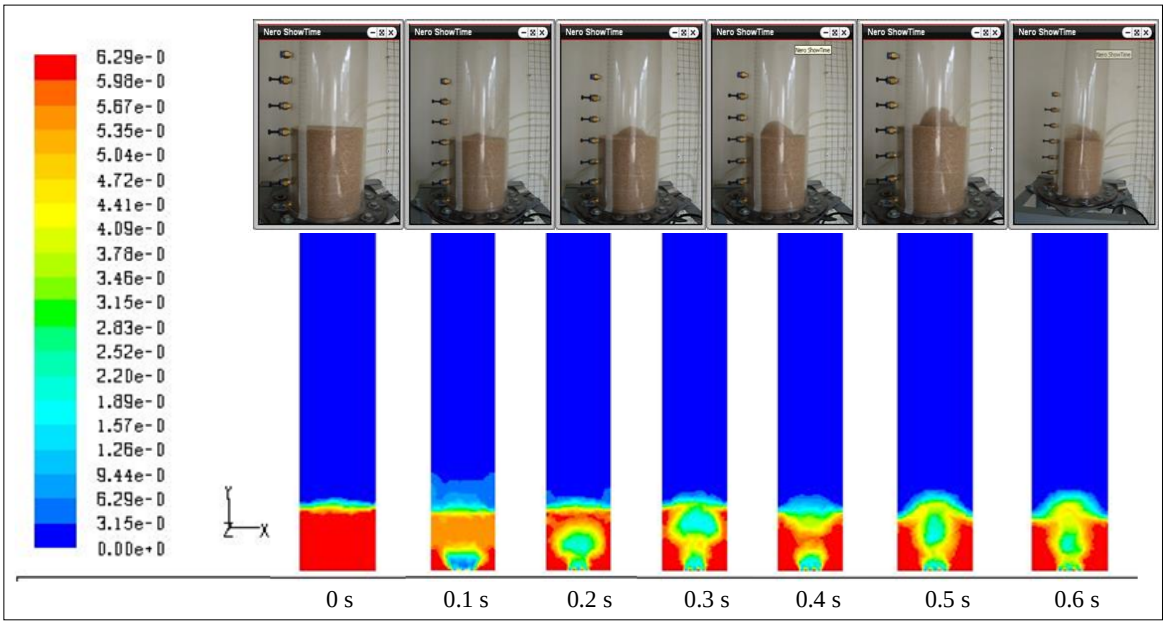

Figure 6. Comparison of the bubble movement inside bed zone resulted from experiment and simulation at t = 0-0.6 s.

4.2 Comparison of hydrodynamic behavior obtained from non-simplified and simplified air distributor model

The simulation results in terms of the solid volume fraction which represents the formation and motion of bubbles inside bed zone, the gas-solid flow pattern, and the bed expansion ratio were compared to show the differences of hydrodynamic behavior obtained from non-simplified and simplified air distributor model.

4.2.1 The difference of bubble formation and motion inside bed zone

The beginning of bubble formation and motion inside bed zone of both non-simplified and simplified air distributor model are indicated with solid volume fraction in Figure 7 and Figure 8. Figure 7 shows the differences of solid volume fraction contour, at time of 0 to 0.8 s, obtained from non-simplified and simplified air distributor model. For non-simplified air distributor model, air starts to come out through the 378 air distributing holes around the 9 closed-end nozzles. Due to the less effect of bed weight, more air bubbles occur at the upper part of the nozzles. The small bubbles are formed and grow as ascending toward the bed surface. Bubbles also collide with each other to form larger ones. As the bubbles reach to the bed surface, they burst out. On the other hand, small bubbles are formed near the bottom of the bed for simplified air distributor model, which was designed to be a plate with holes. Larger bubbles were also formed but at time earlier than observed for the non-simplified air distributor model. Both non-simplified and simplified air distributor model show that, when the bubbles reach the bed surfaces, they erupt and splash solids into freeboard. This result in the fluctuation of bed surface observed. However, more fluctuation is observed in non-simplified air distributor model and the cycles of bubble formation and motion are also faster in non-simplified air distributor model.

The solid volume fraction is also plotted with the reactor height for both models at time 0-0.4 s as illustrated in Figure 8. In the non-simplified air distributor model, the bubbles begin to form at the height of 50 mm from the bottom level but a large and rapid fluctuation of bubble volume is found at the upper part of bed zone. On the other hand, for the simplified air distributor model, the bubbles begin to form right from the bottom level and change their volume fraction as ascending to the surface. The bubbles reach faster to the bed surface in non-simplified air distributor model.

4.2.2 The difference of gas-solid flow pattern

Figure 9 compares the results of solid velocity and flow direction inside bed zone of non-simplified and simplified air distributor model during the beginning period of fluidization, i.e. at time of 0.05 and 0.50 s. For non-simplified air distributor model, solids around nozzles zone start to move downward after gas begins to flow through the air distributors as seen in Figure 9 (left) at time of 0.05 s. Higher gas flow preferably happens at the upper part of nozzles due to less solid weight load and as a consequence pushes the solids toward the bottom. As time proceeds, as shown in Figure 9 (left) at time of 0.50 s, the gas flow at the bottom fully develops and pushes the solids from the bottom to move upward creating solid circulation. It is clear that with this air distributor configuration, local solid circulation was also created and helped maximize the bed circulation. The dead space around the bottom zone of fluidised bed could therefore be reduced.

For simplified air distributor model, solids near the bottom get high acceleration due to the action of gas flow inlet, while the solids on the top of the bed move downward by gravity as presented in Figure 9 (right) at time of 0.05 s. As the gas driving force continues further, large solid circulation patterns are created around the lower zone of the bed as illustrated in Figure 9 (right) at time of 0.50 s.

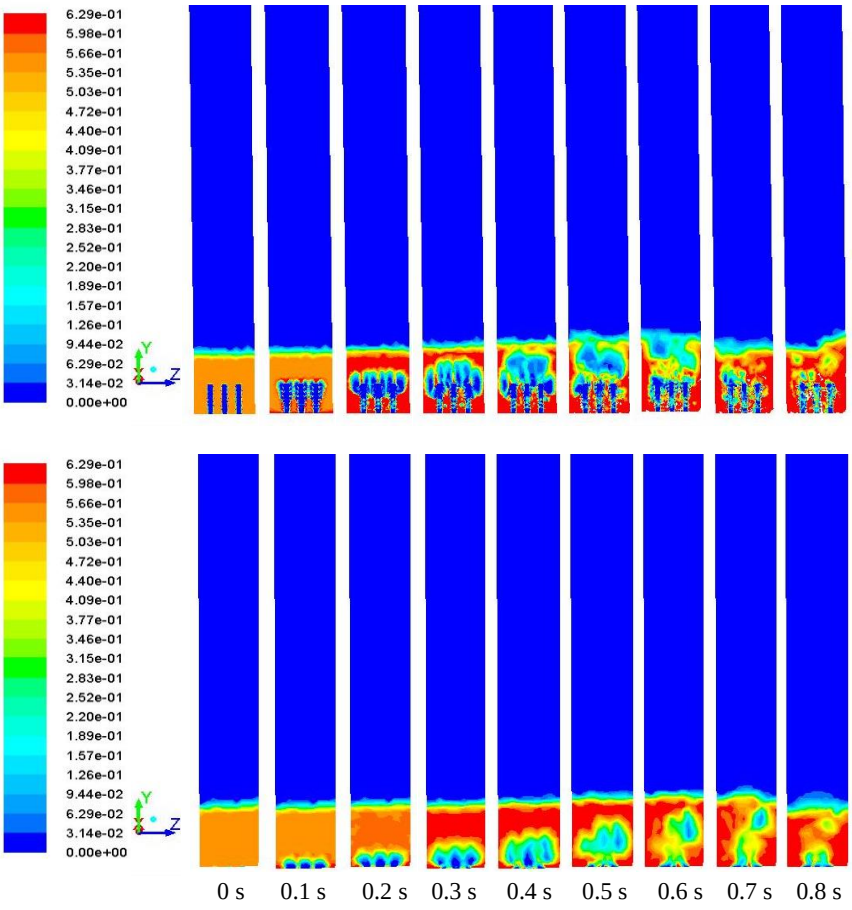

Figure 7. Contour of solid volume fraction at time = 0-0.8 s obtained from non-simplified model (top) and simplified model (below).

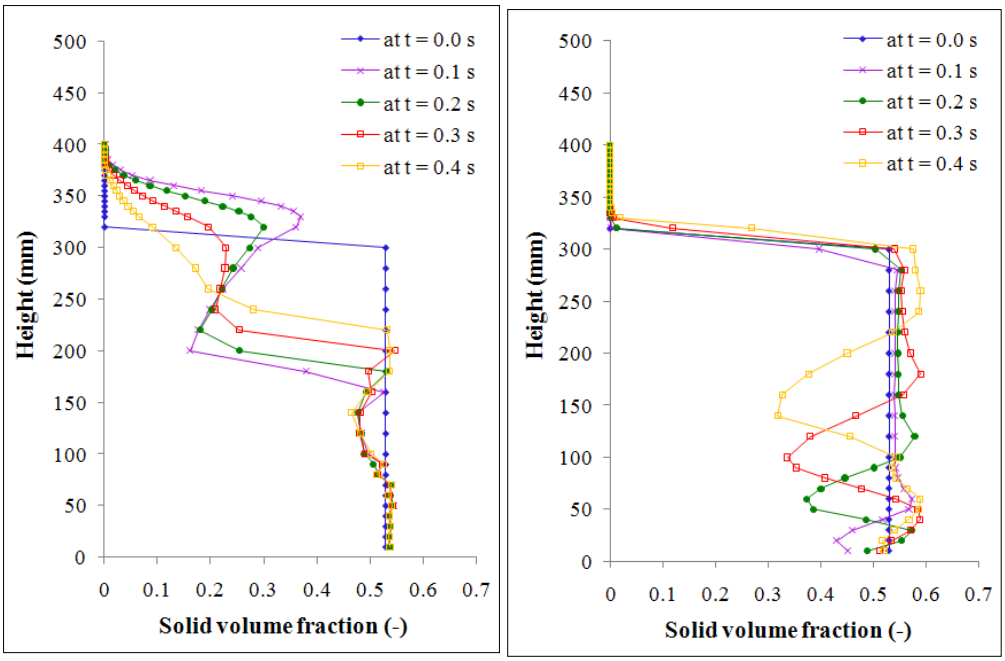

Figure 8. Solid volume fraction along the height of non-simplified model (left) and simplified model (right) at t = 0 to 0.4 s.

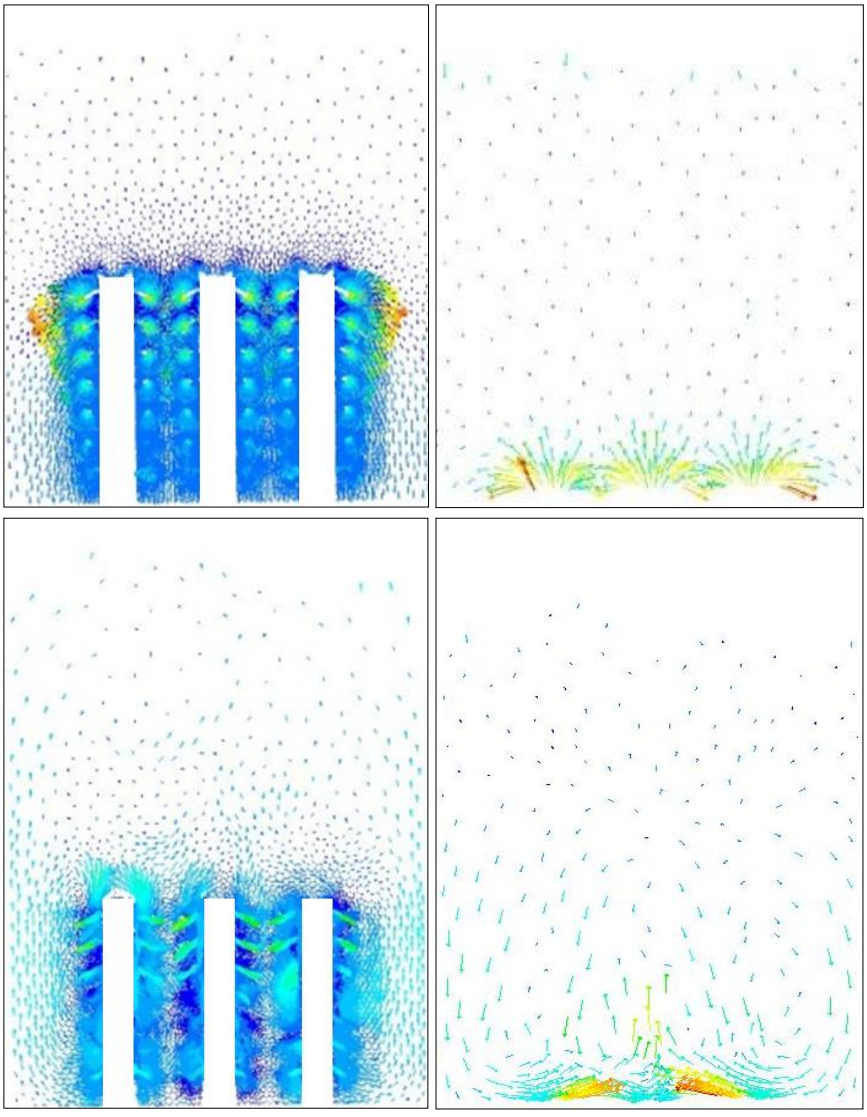

Figure 9. Solid velocity and direction inside bed zone of non-simplified model (left) and simplified model (right).

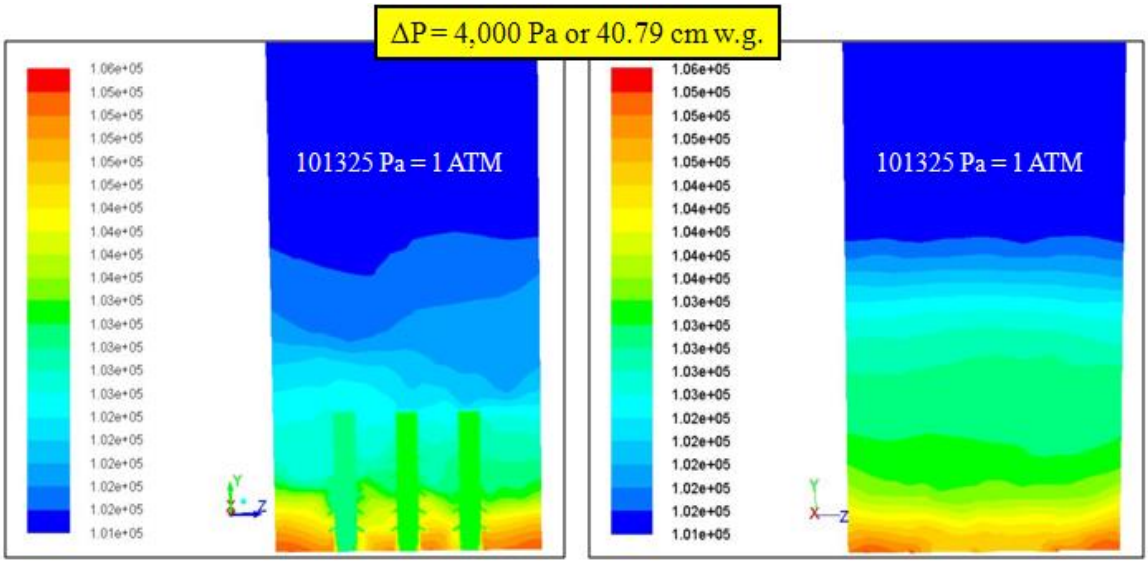

Figure 10. Contour of absolute pressure along the height of non-simplified air distributor model (left) and simplified air distributor model (right) at time = 0.5 s.

4.2.3 The difference of bed expansion ratio

The quasi-steady state bed height obtained from non-simplified model simulation was about 400 mm, while it was about 350 mm in simplified model. Based on the same initial bed height for both non-simplified and simplified model was 300 mm, the bed expansion ratio of non-simplified and simplified air distributor model was 1.33 and 1.16, respectively. This difference indicates that the simulation based on simplified model could underestimate the expansion height of fluidized bed as compared to the non-simplified model which is closer to the actual BFBG.

4.2.4 The difference of absolute pressure profiles along the height of bed zone

The profiles of absolute pressure along the height of bed zone resulted from non-simplified and simplified air distributor model are compared in Figure 10. Although the pressure drop across the bed is similar for both cases at about 40.79 cm w.g., the absolute pressures along the height are different. The simplified air distributor model gives a more constant pressure at all heights, while fluctuations are clearly observed in non-simplified air distributor model, especially in upper zone of the bed. When applying the model under hot flow (reaction considered) mode, this different absolute pressure contour may affect the chemical equilibrium of reactions occurring.

5. Conclusions

The CFD codes of Euler-Euler approach with KTGF were used to develop three-dimensional simulation models to investigate and compare the hydrodynamic behaviors of a bubbling fluidized bed gasifier (BFBG) with non-simplified (actual configuration) and simplified air distributor. To find appropriate input parameters and optional models used, the simulation of a downscale BFB reactor made from acrylic glass was conducted and the experimental results were used for the model validation under cold flow (ambient temperature and non-reactive) condition.

The simulation results show that the presence of non-simplified and simplified air distributor gave somewhat different hydrodynamic behaviors as follows:

• Since the air flow must overcome the complicating air distributor configuration in the non-simplified model, bubble formation (as indicated by the solid volume fraction) was initially slow, but the cycles of bubble formation and motion were faster compared to the simplified air distributor model.

• The more vigorous bubble behavior in the non-simplified model led to a larger fluctuation of bed surface as well as the pressure contour along the bed height.

• With the nozzle-type air distributor configuration, local solid circulation was also created and helped maximize the bed circulation.

• The simplified model could underestimate the expansion height of fluidized bed as compared to the non-simplified model which is closer to the actual BFBG and therefore should be taken with care when fixing the height of fluidized bed required for a particular service.

Acknowledgements

The authors gratefully acknowledge the National Research University Project of Thailand's Office of the Higher Education Commission. The authors would also like to thank Dr. Suthum Patumsawad for the valuable comments on this paper.

References

[1] Yu L, Lu J, Zhang X, Zhang S, Numerical simulation of the bubbling fluidized bed coal gasification by the kinetic theory of granular flow (KTGF), *Fuel* 86 (2007) 722-734.

[2] Yuu S, Umekage T, Johno Y, Numerical simulation of air and particle motions in bubbling fluidized bed of small particles, *Powder Technol* 110 (2000) 158-168.

[3] Kuwagi K, Hoiro M, A numerical study on agglomerate formation in a fluidized bed of fine cohesive particles, *Chem. Eng. Sci* 57 (2002) 4737-4744.

[4] Rhodes MJ, Wang XS, Nguyen M, Stewart P, Liffman K, Use of discrete element method simulation in studying fluidization characteristics: Influence of interparticle force, *Chem Eng Sci* 56 (2001) 69-76.

[5] Limtrakul S, Chalermwattanatai A, Unggurawirote K, Tsuji Y, Kawaguchai T, Tanthapanichakoon W, Discrete particle simulation of solids motion in a gas-solid fluidized bed, *Chem Eng Sci* 58 (2003) 915-921.

[6] Kaneko Y, Shiojima T, Horio M, DEM simulation of fluidized beds for gas-phase olefin polymerization, *Chem Eng Sci* 54 (1999) 5809-5821.

[7] Wang XS, Rhodes MJ, Determination of particle residence time at the walls of gas fluidized beds by discrete element method simulation, *Chem Eng Sci* 58 (2003) 387-395.
[8] Kafui KD, Thornton C, Adams MJ, Discrete particle-continuum fluid modelling of gas-solid fluidised beds, *Chem Eng Sci* 57 (2002) 2395-2410.
[9] Chiesa M, Mathiesen V, Melheim JA, Halvorsen B, Numerical simulation of particulate flow by the Eulerian–Lagrangian and the Eulerian–Eulerian approach with application to a fluidized bed, *Comput Chem Eng* 29 (2005) 291-304.
[10] Gera D, Gautam M, Tsuji Y, Kawaguchi T, Tanaka T, Computer simulation of bubbles in large-particle fluidized beds, *Powder Technol* 98 (1998) 38–47.
[11] Ding J, Gidaspow D, A bubbling fluidization model using kinetic theory of granular flow, *AlChE Journal* 36 (1990) 523-538.
[12] Gamwo IK, Soong Y, Lyczkowski RW, Numerical simulation and experimental validation of solids flows in a bubbling fluidized bed, *Powder Technol* 103 (1999) 117-129.
[13] Gidaspow D, *Multiphase Flow and Fluidization: Continuum and Kinetic Theory Descriptions* (1994) 1st ed.; Academic Press, New York.
[14] Enwald H, Almstedt AE, Fluid dynamics of a pressurized fluidized bed: comparison between numerical solutions from two-fluid models and experimental results, *Chem Eng Sci* 54 (1999) 329-342.
[15] Oevermann M, Gerber S, Behrendt F, Euler-Lagrange/DEM simulation of wood gasification in a bubbling fluidized bed reactor, *Particuology* 7 (2009) 307-316.
[16] Gerber S, Behrendt F, Oevermann M, An Eulerian modeling approach of wood gasification in a bubbling fluidized bed reactor using char as bed material, *Fuel* 89 (2010) 2903-2917.
[17] Chalermsinsuwan B, Gidaspow D, Piumsomboon P, Two- and three-dimensional CFD modeling of Geldart A particles in a thin bubbling fluidized bed: Comparison of turbulence and dispersion coefficients, *Chem Eng J* 171 (2011) 301-313.
[18] Papadikis K, Gu S, Bridgwater AV, CFD modeling of the fast pyrolysis of biomass in fluidise bed reactors. Part B Heat, momentum and mass transport in bubbling fluidized beds, *Chem Eng Sci* 64 (2009) 1036-1045.
[19] Sofialidis D, Faltsi O, Simulation of biomass gasification in fluidized beds using computational fluid dynamics approach, *Original Scientific Paper* 5 (2001) 95-105.
[20] Kaewluan S, Pipatmanomai S, *Preliminary Study of Rubber Wood Chips Gasification in a Bubbling Fluidised-Bed Reactor: Effect of Air to Fuel Ratio* (2007) Proceedings of the PSU-UNS International Conference on Engineering and Environment, Phuket, Thailand, May 10-11, 2007.
[21] Kaewluan S, Pipatmanomai S, Gasification of high moisture rubber woodchip with rubber waste in bubbling fluidized bed, *Fuel Process Technol* 92 (2011) 671-677.
[22] Singh RK, Suryanarayana A, Roy GK, Prediction of bed expansion ratio for gas-solid fluidization in cylindrical and non-cylindrical beds, *J Inst Eng (India), Chem Eng Div* 79 (1999) 51-54.
[23] Gidaspow D, Jiradilok V, *Computational Techniques: The Multiphase CFD Approach to Fluidization and Green Energy Technologies* (2009) Nova Science Publishers Inc., New York, pp. 307-349.
[24] Yurong H, Huilin L, Qiaoqun S, Lidan Y, Yunhua Z, Gidaspow D, Bouillard J, Hydrodynamics of gas-solid flow around immersed tubes in bubbling fluidized beds, *Powder Technol* 145 (2004) 88-105.
[25] Lun CKK, Savage SB, Jeffrey DJ, Chepurniy N, Kinetic theories for granular flow: inelastic particles in Couette flow and slightly inelastic particles in a general flow field, *J Fluid Mech* 140 (1984) 223-256.
[26] Jenkins J, Savage S, A theory for the rapid flow of identical smooth nearly elastic spherical particles, *J Fluid Mech* 130 (1983) 187-202.
[27] Huilin L, Gidaspow D, Bouillard J, Wentie L, Hydrodynamic simulation of gas–solid flow in a riser using kinetic theory of granular flow, *Chem Eng J* 95 (2003) 1-13.
[28] Gunn DJ, Transfer of heat or mass to particles in fixed and fluidized beds, *Int J Heat Mass Transfer* 21 (1978) 467-476.
[29] McKeen T, Pugsley T, Simulation and experimental validation of a freely bubbling bed of FCC catalyst, *Powder Technol* 129 (2003) 139-152.
[30] van Wachem BGM, Schouten JC, van den Bleek CM, Comparative analysis of CFD models of dense gas-solid systems, *AIChE J* 47 (2001) 1035-1051.
[31] Benyahia S, Syamlal M, O'Brien TJ, Evaluation of boundary conditions used to model dilute, turbulent gas/solids flows in a pipe, *Powder Technol* 156 (2005) 62-72.
[32] Almuttahar A, Taghipour F, Computational fluid dynamics of high density circulating fluidized bed riser: study of modeling parameters, *Powder Technol* 185 (2008) 11-23.
[33] Yang WC, Particle segregation in gas-fluidized beds, *Encyclopedia of Fluid Mechanics* 4 (1986) 817-852.

